(Received 24 December 2024, Accepted 12 June 2025, Scheduled 4 August 2025)

Limitations of Low-Frequency Magnetic Field Immunity Testing with Small Radiating Loop

Yasaman Ardeshirpour[1, *], Joshua Guag[1], and Howard Bassen[2]

[1] *Office of Science and Engineering Laboratories, Center for Devices and Radiological Health U.S. Food and Drug Administration, Silver Spring, MD, USA*
[2] *Chevy-Chase, MD, USA*

ABSTRACT: Use of a small radiating loop (6 cm radius) is recommended in EMC standards (Mil-Std-461G:2015(RS101) and IEC 61000-4-39:2017) for immunity testing with low-frequency magnetic fields. We investigated the limitations of this method using finite-element simulations. We studied the effects of fields from radiating loops with different radii and their induced voltages in different radius receiver loops that represented wiring of equipment under test (EUT). We also studied the windowing-method recommended in those standards. It involves positioning the loop successively over all locations on each face of the EUT. Our results show that this radiating loop can only simulate exposure to larger real-world EM fields when the EUT's wiring area is smaller than the radiating loop. Another limitation is that the magnetic field from the radiating loop drops significantly with distance perpendicular to the loop surface. Therefore, the windowing-method with a small radiating loop is only suitable for simulating exposures to real-world sources with fields that do not extend a large distance from the loop. In addition, the field distribution (width and depth) of the real-world EM source must be accounted for before deciding to use a small radiating loop for immunity testing of an EUT.

1. INTRODUCTION

Electromagnetic compatibility (EMC) immunity testing of electronic devices, including medical devices, is conducted to determine whether devices can withstand electromagnetic disturbances in their environment of use including electromagnetic fields from common electromagnetic (EM) emitters in those environments. EMC immunity tests could help to ensure the safe and effective performance of medical devices.

Many sources of potential electromagnetic interference emit low-frequency magnetic fields (e.g., 9 kHz to 150 kHz) that are confined to the immediate vicinity of their radiating coils, like small inductive consumer wireless power transfer systems [1]. In contrast, large intentional radiators such as walk-through metal detectors and electronic article surveillance (anti-theft) systems have one or two panels with multiple large coils that emit strong magnetic fields. Those intentionally large radiators generate emissions that cover a wide spatial volume, in order to perform their intended function. They can expose "victim" devices at significantly greater distances, and they are capable of exposing devices with large susceptible circuitry and wiring volumes [2–7]. It is challenging to perform EMC testing of electronic devices to determine their susceptibility to those intentional large radiators as well as unintentional radiators that emit magnetic fields with wide spatial distributions.

One of the recommended immunity test methods for low-frequency magnetic fields used in close proximity of devices is the "windowing method". This method uses a small radiating loop based on the Mil-Std-461G:2015 (test RS101) and IEC 61000-4-39:2017 standards [8, 9], which designate repositioning the loop successively over each specified area/location (window) on each face and connector of the equipment under test (EUT). For magnetic field immunity testing at 9 kHz to 150 kHz, clause 6.1.2 of IEC 61000-4-39:2017 recommends using a radiating loop with a radius of 6 ± 0.5 cm, made of a coil with 20 turns of wire with a wire radius of 0.1 cm. The unperturbed magnetic field of the radiating loop at a 5 cm distance from the plane of the loop should be $H = 75.6 \times I$ (A/m) equivalent to a flux density of $B = 9.5 \times 10^7$ pT/A $= 95$ μT/A. This is similar to testing with a radiating loop in MIL-STD-461G:2015 (test RS101). The IEC 61000-4-39:2017 standard recommends scanning each window face of the device with a radiating loop at a 5 cm distance with maximum size of 10×10 cm^2.

In this paper, we report our investigations on the limitations of testing immunity to various magnetic field sources using a small magnetic field radiating loop as specified in the above EMC standards. To do this we evaluated the magnetic field distribution produced by small radiating loops specified in these standards and the resulting induced voltages on different radius receiver loops (simulating victim devices). We used simulations with finite-element method software to study the magnetic field generated by a single radiating loop. In addition, we evaluated the field distributions from larger radius loops, and the appropriate use of both types of radiating loops that can be used for immunity testing.

Section 2 of this article provides the simulation and experimental methods, and Section 3 presents the results, discussion

* Corresponding author: Yasaman Ardeshirpour (yasaman.ardeshirpour@fda.hhs.gov).

of the results, and limitations of the windowing method with a small radiating loop. Conclusion is provided in Section 4.

2. METHODS

2.1. Simulations

For simulations presented in this paper, we used the AC/DC module of COMSOL Multiphysics 6.2 software (COMSOL AB, Sweden) to model radiating loops with different radii alongside various radius receiver loops. This was done to investigate the low-frequency magnetic field distribution of the radiating loops and the voltage induced in various receiver loops via those magnetic fields. We also compared the results with an ideal uniform magnetic field with the same targeted magnetic flux (which could approximately represent the fields produced by a large radius Helmholtz coil). Each section below describes different parts of the simulation models.

2.1.1. Radiating Loop

For our simulations, we varied the radiating loops' radii from 4 to 10 cm with 1 cm step size, and from 10 to 30 cm with 5 cm step size. The radiating loop was oriented, so its broad surface was in XY plane as shown in Fig. 1. Each coil consisted of 20 turns of wire with a wire radius of 0.1 cm.

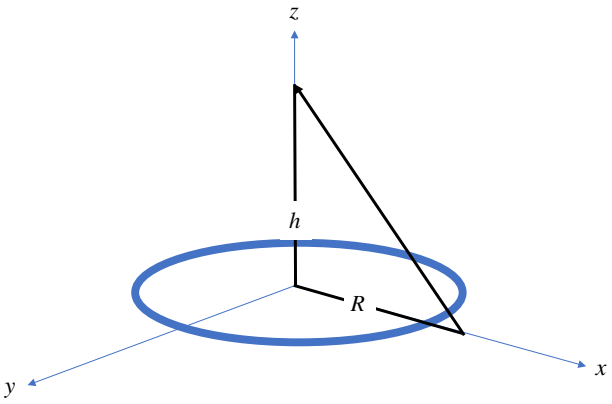

FIGURE 1. Radiating loop (in XY plane).

The current in each coil (Table 1) was calculated with Equation (1) [10], to create a magnetic field with a flux density of $B = 9.5 \times 10^7$ pT $= 95$ μT at 5 cm from the center of the loop in the Z-direction, as specified in the standards under discussion [8, 9].

$$B = \frac{\mu I N R^2}{2\left(h^2 + R^2\right)^{3/2}} \tag{1}$$

In Equation (1), B is the magnetic flux density; h is the distance from the center of the loop in a perpendicular direction (Z-axis); R and N are the radiating loop's radius and number of turns of wire, respectively; I is the current inside the loop; and μ is the permeability of the surrounding media (air).

The windowing method in the IEC 61000-4-39:2017 standard is recommended for a frequency range of 9 kHz to 150 kHz, so we chose an arbitrary frequency of 14 kHz for all simulations. This paper deals with coils whose radii are much smaller than the wavelength of the frequency that excites them; therefore, the frequency of the current in the coil does not affect the radiated field from the coil.

TABLE 1. Required current in a radiating loop to produce a magnetic flux density of 95 μT at $x = 0$, $y = 0$, $z = 5$ cm from the center of different radius radiating loop at $x = 0$, $y = 0$, $z = 0$ (Fig. 1).

Radiating loop radius (cm)	Radiating loop current (A) based on Equation (1)
4	1.24
5	1.07
6	**1.00**
7	0.98
8	0.99
9	1.02
10	1.06
15	1.33
20	1.66
25	2
30	2.36

2.1.2. Receiver Loop

The receiver loops were modeled as a circuit consisting of a circular wire configuration with a radius ranging from 4 to 10 cm with 2 cm step size. They represented a simple model of a cardiac pacemaker implanted in a patient. We used a single turn of copper wire with a radius of 0.1 cm, covered with an insulation shield with thickness of 0.1 cm to represent the implant's "lead". One end of the wire was connected to an electronics box whose internal impedance (simulated by a lumped element) was 100 Ω. The other side of the wire was connected to a resistor (a lumped element) with an impedance of 500 Ω, representing a patient's tissues surrounding the tip of the wire lead [11]. The electronic box was modeled as a $4 \times 3 \times 1.5$ cm^3 stainless steel box with a thickness of 0.3 cm and filled with air. The insulation shield was used to prevent direct contact of the wire to the body of the electronics box.

Since the relative permeability of tissue is the same as that of free space (μ_0) [12], we assigned the tissue a value of μ equal to μ_0 in our simulations. The receiver wire loop (lead) was surrounded by air, as shown in the receiver loop model in Fig. 2.

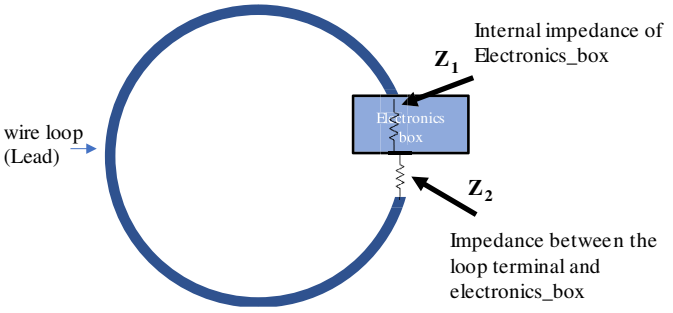

FIGURE 2. Receiver loop model.

This simplified configuration was intended to enable our results to be applied to other types of electronic devices.

2.1.3. Calculation of Induced Voltage in the Receiver Loop

To calculate the induced voltages from the radiating loop across the tissue (media) and electronics box impedances, the radiating and receiver loops were both placed parallel in XY planes with a separation distance of 5 cm in the Z-direction (Fig. 3). This distance is specified in Mil-Std-461G:2015 (test RS101) and IEC 61000-4-39:2017 standards for a 6 cm radius radiating loop. The receiver and radiating loops were placed in a block air media length 20 times larger than the radius of the largest loop.

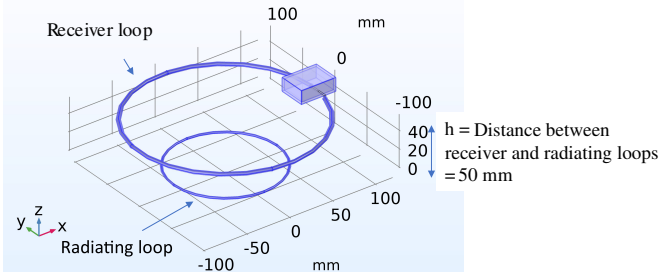

FIGURE 3. Receiver and radiating loops positions.

Since lead has a very high conductivity, the total induced voltage in the receiver loop was considered equal to the sum of induced voltages across the electronics box and the tissue media impedances.

The frequency domain magnetic field solver in the AC/DC module was used for the electromagnetic field simulation. The predefined finer mesh was used for the air media, and extra-fine or extremely fine mesh was used for all other geometries. The mesh size was decreased till changing the mesh size further did not change the simulation results. Relative error of 0.001 was selected for the finite-element solver. The convergence curve was monitored to ensure the convergency of the solver.

2.1.4. Magnetic Fields Distribution of Radiating Loop

To calculate the field distribution of the radiating loops, we evaluated the depth and width of the magnetic field distribution of radiating loops with different radii. We used perpendicular (Z) direction from the center of the radiating loop ($x = 0$, $y = 0$) in YZ plane, to calculate the depth of the magnetic field where the flux density was 50% of the targeted flux density value (i.e., 95 µT). For the width of magnetic fields at receiver location, we used the distance between the two points along the Y-axis at ($x = 0$, $z = 5$ cm) where the flux density drops to 50% of the 95 µT.

2.1.5. Windowing Method

To study the windowing method as recommended in IEC 61000-4-39:2017 standard, we moved different radius radiating loops to various locations with respect to a 10 cm radius receiver loop in the direction of the Y-axis, with a constant separation distance of 5 cm in Z-direction. We calculated the total induced voltage in the receiver loop ($V_{\text{tissue}} + V_{\text{electronics box}}$) by the magnetic field of the radiating loops. In addition, we calculated the total induced voltage in the receiver loop by an ideal uniform magnetic field in Z-direction with a magnitude of 95 µT.

2.2. Experiments

To confirm the simulation results with experimental data, we used a 19 cm radius (15-inch diameter) Helmholtz coil to generate a uniform magnetic field in the area of the receiver loops. Additionally, we used a commercial 6 cm radius coil with 20 turns (FESP 5132, Schwarzbeck Mess-Electronik, Germany) and a custom-made 10 cm radius coil with 20 turns. A sinusoidal signal with a frequency of 14 kHz was fed to each coil, generated by an Agilent 33220A 20 MHz Function/Arbitrary Waveform Generator (Keysight, USA), connected to a Clarke-Hess Transconductance Amplifier, Model 8100 (Clarke-Hess, USA). The magnetic field at the center of the Helmholtz coil was measured using a 3 cm^2 Narda Probe ELT-400 (Narda-sts, USA). For the 6 cm and 10 cm radius coils, the total magnetic field at 5 cm above their centers was measured using one of the 3-axis magnetic sensors (with a loop size of 1 cm^2) from the MAGPy version 2 (SPEAG Inc., Switzerland), integrated with the DASY6 robotic arm system (SPEAG Inc., Switzerland).

Custom-made receiver loops were made with 4-, 6-, 8-, and 10-centimeter radii and were connected with a twisted cable to an Agilent Technologies DSO9104A oscilloscope (Keysight, USA). The twisted cables were positioned perpendicular to the radiating coils surface to minimize the induced voltage in the twisted connecting wires. The induced voltage measured from the receiver loops was normalized to the ratio of 95 µT magnetic field used in simulation, and magnetic field measured at 5 cm above the center of the transmitter coils or inside the Helmholtz coil, to facilitate comparison with the simulation results. We measured the induced voltages, 3 times by rotating the receiver loops parallel over radiating loop or inside the Helmholtz coil about 120 degrees to test the results repeatability.

3. RESULTS AND DISCUSSION

3.1. Magnetic Fields Distribution of Radiating Loops with Different Radii

We studied the magnetic fields generated by different radius radiating loops to evaluate the extent of their magnetic field (Fig. 4(a)), both in the direction perpendicular to the broad surface of the loop along the Z-axis (depth) and for the width of the field 5 cm from the loop's surface in the XY plane (at the receiver plane).

A 6 cm radius coil (as specified in the Mil-Std-461G:2015 and IEC 61000-4-39:2017 EMC standards) had a depth of 7.8 cm from radiating loop (or 2.8 cm from receiver loop), while a 30 cm radius coil had a depth of 23.8 cm from radiating loop (or 11.8 cm from receiver loop) (Fig. 4(b)). These results show that a 6 cm radius radiating loop produces magnetic fields that are highly confined to the immediate region of the loop and can

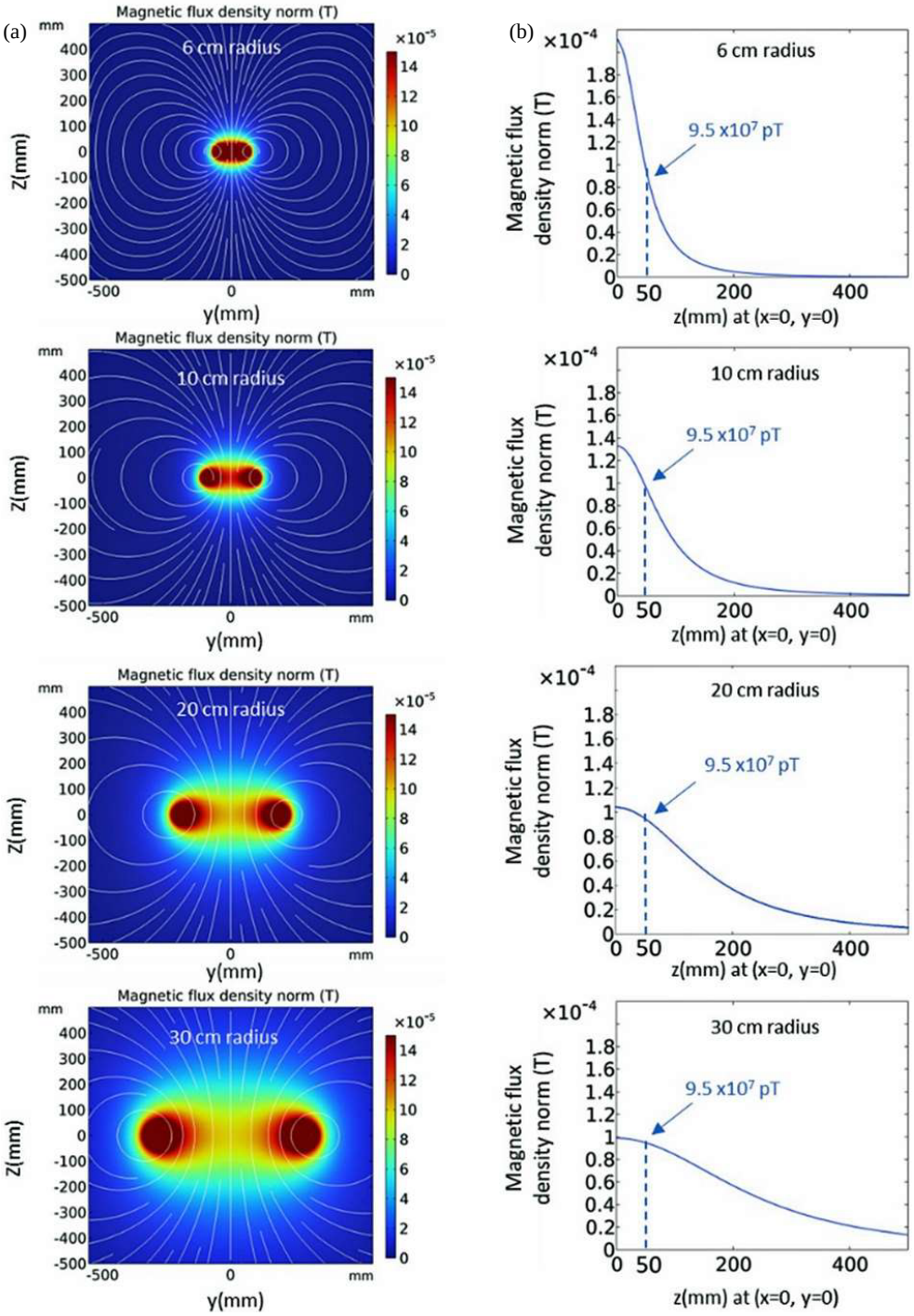

FIGURE 4. Depth of magnetic field distribution of radiating loops with different radii (a) in YZ cross section, (b) at different distances along the Z-axis, perpendicular to the center of the coil ($x = 0, y = 0$).

mainly expose electronic circuits and wiring that are near or on surface of the victim device under test.

The width for the 6 cm loop was 15 cm, and 80 cm for the 30 cm loop (Fig. 5). This shows that immunity testing with a 6 cm radius loop is primarily effective when all the vulnerable circuitry and wiring are in the area directly under the radiating loop.

3.2. Induced Voltage in Different Radius Receiver Loops from the Magnetic Field Generated by Different Radius Radiating Loops

We calculated the induced voltage in different radius receiver loops from different radius radiating loops and ideal uniform magnetic field in Z-direction with a magnitude of 95 μT (Figs. 6 and 7). These fields were generated by a radiating loop, located parallel to the receiver loop at a separation

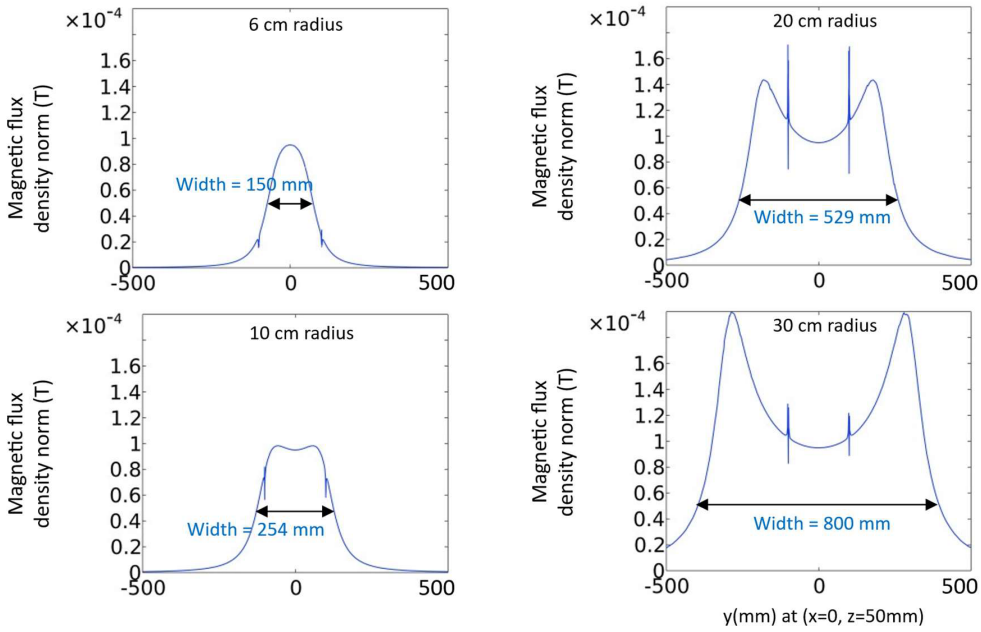

FIGURE 5. Magnetic field values along the Y-axis at ($x = 0$, $z = 5$ cm) for different radiating loop radii. The width is defined as the location where the flux density drops to 50% of the 95 µT for each plot. The vertical lines in the graphs mark the location of the 10 cm radius receiver metal loop (the center of receiver loop is located at $x = 0$, $y = 0$, and $z = 5$ cm). The center of radiating loop is located at $x = 0$, $y = 0$, and $z = 0$ cm.

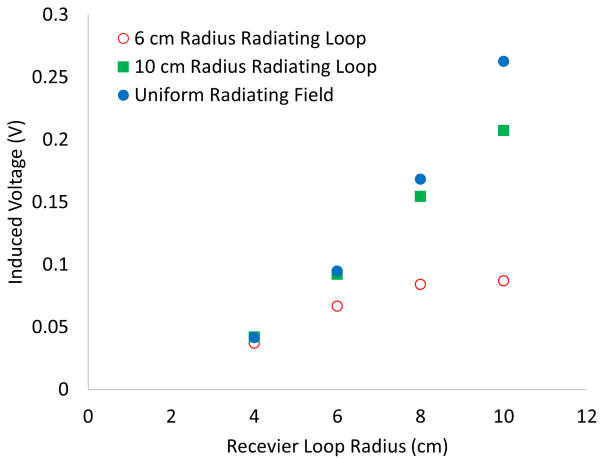

FIGURE 6. The total induced voltage in different radius receiver loops from a 6 cm and a 10 cm radius radiating loop (red circles and green squares). The blue circles show the total induced voltage in receiver loops from an ideal uniform magnetic field in the Z-direction with a magnitude of 95 µT.

distance of 5 cm. The centers of the radiating and receiving loops were aligned and were centered on the Z-axis.

For receiver loops (simulating an EUT) with a larger radius than 6 cm, the following occurs (Fig. 6). When exposed to fields from the 6 cm radiating loop, the voltage induced in the receiver loops increases in proportion to the receiver loops' radius, but reaches an asymptote when the radius of the receiver loops is greater than 8 cm. However, the voltage induced in these receiver loops is small compared to the induced voltage from radiating loops with larger radii or an ideal uniform magnetic field. The results also show that the voltages induced by the 6 cm radiating loop in a 10 cm radius receiver loop are about 3 times smaller than the voltages induced by a 30 cm radiating loop (Fig. 7).

The results for a 6 cm radius radiating loop (Figs. 6 and 7), show that only receiver loops with a smaller radius than 6 cm had an induced voltage equal to the induced voltage from larger radiating loops or an ideal uniform magnetic field with the same targeted flux density value. Therefore, if the 6 cm radiating loop is used to simulate the exposure of EM emitters with larger coils, using 6 cm radius radiating coil is only effective when the receiver loop is smaller than the radiating loop.

To confirm our simulation results, we conducted an experiment with the same setup for Fig. 6. Fig. 8 shows the results for Helmholtz coil, 6 and 10 cm radius radiating loops with 20 turns. The difference between the simulated and experimental results for the 6 cm and 10 cm radiating loops can be attributed to variations between the simulated and actual radiating loops, inaccuracies in the magnetic field sensor and the distance between the receiver and the radiating loop. Nevertheless, the experiments demonstrated consistent trends with the simulation data.

3.3. Windowing Method

We also studied immunity testing with the windowing method that involves positioning the radiating loop successively over all locations on each face of the EUT. We observed the changes in the voltage induced in 5 cm and 10 cm radius receiver loops by the magnetic field emitted from a 6 cm radius radiating loop. The induced voltage was the highest when the center of radiating and receiver loops were aligned and decreased as the center of radiating loop was moved away from the center of the receiver loop. We also compared the results of a 6 cm radius ra-

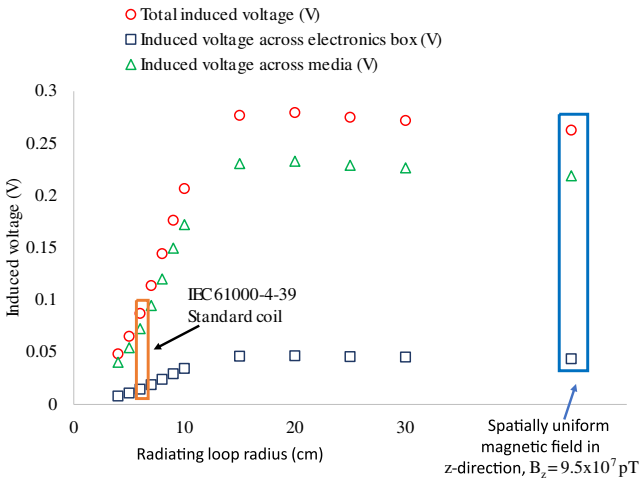

FIGURE 7. Voltages induced in a 10 cm radius receiver loop circuit across the electronics box (blue square markers), across the tissue media (green triangle markers), and across combined both elements (red circles) for radiating loops with different radii. The orange rectangle shows voltage induced from the 6 cm radius radiating loop.

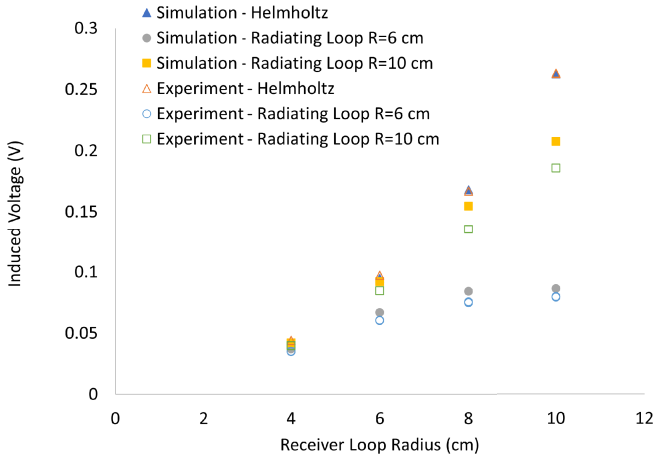

FIGURE 8. Comparison of measurement and simulation results for the total induced voltage in different radius receiver loops at 5 cm distance from a 6 cm and a 10 cm radius radiating loop, and a uniform magnetic field generated by a Helmholtz coil.

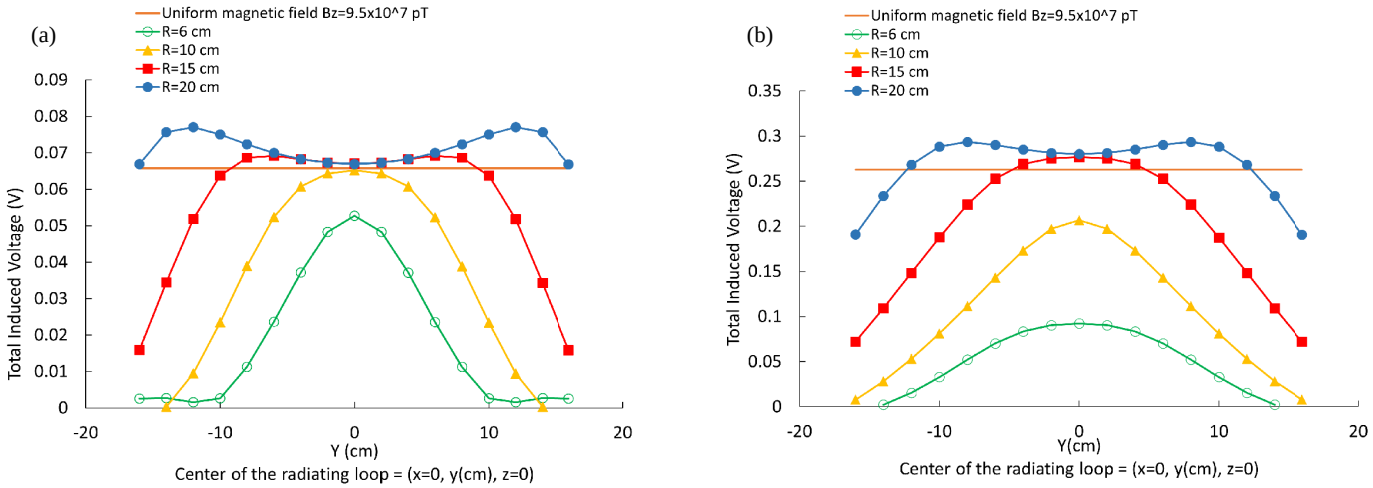

FIGURE 9. Windowing method — Total induced voltage in a (a) 5 cm, (b) 10 cm radius receiver loop from different radius radiating loops. The horizontal axis of the graph shows the center location of the radiating loop. The receiver loop center was at ($x = 0$, $y = 0$, $z = 5$ cm). The straight horizontal orange line shows the total induced voltage in the receiver loop from a uniform magnetic field in Z-direction with magnitude of 95 µT. The higher induced voltages for 15 and 20 cm radius radiating coils from uniform magnetic field are due to higher lobes of the magnetic fields of those coils (the field for 20 cm radius radiating loop is shown in Fig. 5).

diating loop with larger radius radiating loops, and an ideal uniform magnetic field with the same targeted flux density value (Figs. 9(a) and 9(b)).

Based on our simulation, achieving the same induced voltage in a receiver loop with 5 cm radius requires the magnetic field generated by 6 cm radius radiating loop (when aligned with the center of the receiver loop at 5 cm distance) to be about 20% more than that of a uniform magnetic field. For a 10 cm radius receiver loop, that required increase is about 65%.

These results show that using a 6 cm radius loop for simulating exposures of larger EM radiating loops is primarily suited for immunity testing of devices with small thicknesses and with all vulnerable circuity and wiring contained in an area equal or smaller than the radiating loop's radius.

4. CONCLUSION

In this paper, we have studied the limitation of windowing method using low-frequency small magnetic coil for simulating the real-world EM emitters. We used finite element software to study the magnetic fields generated by different radius radiating loops and the voltage they induced in different radius receiver loops. Our results indicate that using a 6 cm radius radiating loop to test EUTs, as recommended in Mil-Std-461G:2015 (test RS101) and IEC 61000-4-39:2017 standards, has limitations. Specifically, this method is effective for assessing susceptibility to real-world radiating emitters with shallow, highly localized magnetic fields with dimensions equal to or smaller than the 6 cm loop. However, using the 6 cm loop is not suitable by

default for evaluating susceptibility to real-world emitters with deep and/or large fields relative to a 6 cm area, without considering the structure of the EUT like its thickness and area of its susceptible circuits and wires.

DISCLAIMER

The mention of commercial products, their sources, or their use in connection with material reported herein is not to be construed as either an actual or implied endorsement of such products by the Department of Health and Human Services.

REFERENCES

[1] Zhang, Z., H. Pang, A. Georgiadis, and C. Cecati, "Wireless power transfer — An overview," *IEEE Transactions on Industrial Electronics*, Vol. 66, No. 2, 1044–1058, Feb. 2019.

[2] Leitgeb, N., F. Niedermayr, and C. Fuchs, "Impact of a radio frequency electronic article surveillance (EAS) system on active implants," *Journal of Electromagnetic Analysis and Applications*, Vol. 4, No. 9, 353–357, 2012.

[3] Casamento, J., "Characterizing electromagnetic fields of common electronic article surveillance systems," *Compliance Engineering*, Vol. 16, No. 6, 42–52, 1999.

[4] Boivin, W., J. Coletta, and L. Kerr, "Characterization of the magnetic fields around walk-through and hand-held metal detectors," *Health Physics*, Vol. 84, No. 5, 582–593, 2003.

[5] Research reports on nuclear safety and radiation protection, supplementary analysis of RFID exposure data technologies from FV 36090S80002 and studies electronic article surveillance security systems, project 3612S8004, in German (urn:nbn:de:0221-2014080611454, 2014).

[6] Guag, J., B. Addissie, and D. Witters, "Personal medical electronic devices and walk-through metal detector security systems: Assessing electromagnetic interference effects," *Biomedical Engineering Online*, Vol. 16, 1–15, 2017.

[7] Seidman, S. J., W. Kainz, J. Casamento, and D. Witters, "Electromagnetic compatibility testing of implantable neurostimulators exposed to metal detectors," *The Open Biomedical Engineering Journal*, Vol. 4, 63–70, 2010.

[8] International Electrotechnical Commission (IEC), "Electromagnetic compatibility (EMC) — Part 4-39: Testing and measurement techniques — Radiated fields in close proximity — Immunity test, IEC 61000-4-39," 2015.

[9] Department of Defense Interface Standard, "Requirements for the control of electromagnetic interference characteristics of subsystems and equipment, MIL-STD-461G," 2015.

[10] Cheng, D. K., *Field and Wave Electromagnetics*, 2nd ed., Pearson Education Limited, Boston, MA, USA, 1989.

[11] International Organization for Standardization (ISO), "Implants for surgery — Active implantable medical devices — Part 3: Implantable neurostimulators," ISO-14708-3:2017.

[12] Seo, J. K., E. J. Woo, U. Katscher, and Y. Wang, *Electro-Magnetic Tissue Properties MRI*, 296, Imperial College Press, United Kingdom, 2014.